

Dear Editor,

We are grateful to the reviewers for their constructive comments that we believe have helped us to strengthen the manuscript. *Major changes to the text are shown in blue in the manuscript.* Below we include the original review, and we respond to each comment line-by-line. Original reviewer's comments are shown in black, and *our response in blue.*

Sincerely,
Juying Warner

Department of Atmospheric & Oceanic Science
University of Maryland
Email: juying@atmos.umd.edu

Reviewer #1 (Comments to Author):

In this manuscript, observations made from the Atmospheric Infrared Sounder (AIRS) in the spectral region between 860 and 967 cm^{-1} are used in a forward model to deduce NH_3 concentrations, averaging kernels and degrees of freedom for signal. As the authors note, other satellite-borne IR spectrometers, including IASI and TES, also provide retrievals for ammonia on a global scale. The challenge for all such measurements is that NH_3 mixing ratios are typically at a maximum within tens or hundreds of meters of the Earth's surface, whereas the retrieval is most sensitive at higher altitudes. Further compounding the challenge is that chemical transport models often struggle to reproduce the diel behaviour of NH_3 , and its vertical distribution in the atmosphere in the few regions where in situ measurements are available for comparison.

We agree with the reviewer that it is challenging to measure NH_3 on a global scale, which makes it more valuable to use satellite products. We do not agree with the statement that the retrieval is most sensitive at higher altitudes, because the spectral range we use is in the atmospheric window region, and with NH_3 concentration typically at a maximum within tens or hundreds of meters of the Earth's surface (as stated by the reviewer), we can see through the "clean" atmospheric column into the lower troposphere with best sensitivity at 918 hPa.

Throughout the paper, the authors conflate high observed volume mixing ratios (VMRs) retrieved at 918 hPa with high emissions at that location. It is not necessarily the case that high VMRs observed aloft correspond to high emissions directly below the retrieval, especially given the importance of wildfires to high signal at 918 hPa. Even if the VMR is related to local emissions, the retrieved quantity will also depend on the degree of vertical mixing and the impacts of sinks such as deposition and gas-particle partitioning. I think the language used in the manuscript is somewhat misleading since it implies that elevated VMRs at 918 hPa are uniquely associated with elevated emissions. Since the authors restrict themselves to only three pollution scenarios to serve as a priori profiles, it may be a

convenient shorthand but it can lead to misleading statements about the interpretation of the retrievals.

This is our oversight. We have carried out model studies over China (not shown) that demonstrate the NH₃ emissions and the concentrations are linearly correlated, however, not at the same rate. We have made correction to change the term ‘emission’ into ‘concentration’ in all the relevant locations in the manuscript.

In Section 3, the authors use in situ measurements from the DISCOVER-AQ field campaign in California during the winter of 2013 to evaluate retrieval profiles. These aircraft profiles are useful, in that they occur in a significant source region, which may be expected to correspond to the ‘high pollution’ a priori. On the other hand, there is significant heterogeneity, with individual aircraft profiles corresponding to the same satellite retrieval measuring mixing ratios that differ by an order of magnitude close to the surface. This section ends without a clear statement about the quality of the retrieval methodology, as evaluated using this comparison.

We added the following sentence at the end of the section: “Nonetheless, the vertical profiles show good agreement (~5 – 15%) between AIRS NH₃ and the in situ profiles in the examples given above.”

In Section 4, the authors apply the methodology to the globe from 2002-2015. As they state, interpreting the analysis requires not only consideration of the average VMR at 918 hPa, but also the frequency of elevated ‘emissions’ (actually VMRs > 1.0 ppbv at 918 hPa), and also the retrieval DOFs. It appears that many of the regions with the highest average VMRs are in places with infrequent occurrences of high emissions, probably related to episodic wildfires. Given that the relationship between VMR at 918 hPa and emission is likely very different for agricultural and wildfire emissions, it becomes challenging to use the retrievals to constrain the global budget of NH₃. Furthermore, the authors state that regions where DOFs are never above 0.1 are excluded from the analysis. But what about regions where DOFs are < 0.1 the majority of the time, but are occasionally impacted by wildfire. Is the average VMR reported for that pixel simply the average of the high signal episodes, or the average of the entire time period, in which case a significant fraction of the time the retrieval is probably indistinguishable from the a priori?

This approach with related thresholds was applied to illustrate where the major global NH₃ sources are; was not intended to constrain the global budget of NH₃. Also once a region is identified as being persistent sources using the frequent occurrences thresholds, we use all data (not just high signal episodes) in the average in that region.

I did not find Figure 6, and the associated discussion to add significantly to the manuscript. It is to be expected that fertilizer use and animal husbandry will dominate ‘persistent sources’ of NH₃ on a global scale, so what new information is gained here?

We intend to show here that our observations are consistent with prior knowledge.

Specific Comments Lines 45-47 – References would be good for these statements, particularly that idea that NH₃ deposition increases emissions of CH₄.

We have added references and modified into the following sentences:

“Ammonia deposition modifies the transport lifetimes, and deposition patterns of sulfur dioxide (SO₂) and nitrogen dioxide (NO_x) (Wang et al., 2008; Henze et al., 2012).

Additionally, ammonia increases the concentrations of the greenhouse gases nitrous oxide (N₂O) (EPA, 2011) and, together with NH₄⁺ content in soils, NH₃ is involved in CH₄ production and release (Fowler et al., 2009).”

Lines 52-72 – In the second paragraph of the introduction, it’s difficult to tell if the authors are stating that they used the NH₃ fields generated in the Park et al., 2004 study, or whether they ran GEOS-Chem themselves using the methods described in Park et al., 2004. Later, it is mentioned that v9-02 was used – this information should be clarified in the introductory paragraph.

We moved the sentence “We used the simulated NH₃ fields from GEOS-Chem as the retrieval a priori for this study.” to the front of the paragraph to clarify the purpose of this model discussion.

Lines 9-99 – This sentence is a bit confusing. Does the ‘both’ in ‘if both are large enough’ refer to the concentrations and thermal contrast, or retrieval and radiative transfer model runs. One assumes the former, but it’s hard to tell from the sentence.

We changed the sentence to “..., if both of the NH₃ concentrations and thermal contrast are large enough, ...”

Line 142 – Sentence refers to the contributions of co-authors Strow and Hannon, but Hannon does not appear in the author list of this manuscript

Changed to co-author Strow and team.

L185-187 Why is the a priori developed for 2003-2012 when it is applied for observations between 2002-2015?

The a priori was developed at the beginning of algorithm development (in 2012), but we extended our data product to current time. A priori information shows our current knowledge of the data range, which has not changed significantly between 2012 and 2015. Therefore, there is no need to update the a priori information as we continue processing new measurements.

L186 and Figure 1. I find the use of ‘level’ for the three different versions of the a priori

somewhat confusing because it makes me think of vertical levels. Perhaps using the term ‘emission scenarios’ instead of ‘emission levels’ would be more clear? Also, it would be interesting to know if the three scenarios differ in terms of shape or just overall levels. This could be shown with an additional panel in which each scenario is shown normalized to the surface concentration.

We changed “levels” to “scenarios”. We used a large number of NH₃ profiles from GEOS-Chem model output to derive the statistic properties of these a priori profiles. The shapes of the three scenarios are different but follow the model property.

L196-198 How significant are the adjustments and extrapolations mentioned here?

It is not possible to measure the near surface high NH₃ values as described by the model, so we modified the a priori profile shape to suit satellite measurements better.

Figure 3 – it’s too difficult to distinguish between the solid and dashed green lines in the figure panels

We changed the green dashed lines to blue.

L 318-320 Can the authors clarify why they excluded the nighttime retrievals carried out at 01:30? Measurements of NH₃ in the residual layer would be valuable.

Additional studies are needed to specifically address NH₃ retrievals at nighttime and will be included in a future publication.

Section 5 - Can the seasonality in the retrievals be uniquely attributed to seasonality in column NH₃ or the VMR at 918 hPa?

The seasonality is for the VMR at 918 hPa.

Technical comments L79 remove ‘the’ before Beijing’

Corrected.

Reviewer #2 (Comments to Author):

The authors of this paper describe the algorithm to derive ammonia from AIRS measurements using inversion theory pioneered by C. D. Rodgers, and present spatial and temporal (in seasonal sense) analysis of global ammonia distributions. This is important work and the paper should be published. The paper, however, could have been better written and data analyzed more thoroughly (e.g., just noting a particular phenomenon and merely speculating the cause is not enough). I have specific comments below that I would like the authors to address. I recommend the publication of the paper after these comments are addressed. The revisions that I am recommending are not major and should not take more than a month or two to implement. I highlight my concerns below:

[We thank Reviewer #2 for providing insightful comments.](#)

The paper needs editorial work. Many blatant errors and sentences with poor word choices are present in the paper and need to be resolved. For example, on page 4, “R’Honi et al. (2013) discussed the exceptional emissions of NH₃ and HCOOH in the 2010 Russian wildfires.” Another example is the reference to 13-yr time period as long-term. It so happens that there is a 13-yr record of AIRS ammonia retrievals. However, that does not define what a long-term record is. Because the 13-yr record is close to a decade, that could be used in a general sense perhaps?

[We changed the first sentence to “R’Honi et al. \(2013\) discussed the elevated concentrations of NH₃ and HCOOH emitted by the 2010 Russian wildfires.” We took out the work longterm and changed the sentence to “Global ammonia sources and variability based on continuous monitoring with longer than a decade record \(13 years\) have not been available.”](#)

Algorithm should be discussed in general terms instead of repeating material from Rodgers book/papers. The methodology should be conceptually explained for ammonia and also other trace gases that are generally simultaneously retrieved inverting hyperspectral infrared radiances.

[We aim to provide details so that the process for the retrieval can be repeated.](#)

Validation of the retrievals is only done for two weeks. I understand that not many ground measurements of ammonia exist but the DISCOVER-AQ field campaign data provided the authors with profiles covering 2-week time period. The comparisons are very encouraging. To explain the differences between retrieved and aircraft observed profiles for some cases, the authors revert to spatial variability of ammonia in a 45-km grid space (aircraft captures that variability but satellites can’t resolve it). It would be nice if the authors can actually demonstrate the spatial variability of ammonia (from models or other ground observations) to explain the usability of AIRS ammonia product. Does this mean that AIRS ammonia retrievals at 45-km resolution (is it larger at scan edges?) are of no use to high resolution air

quality models for forecasting applications? Are the retrievals more useful in regions where spatial variability is not that high? I think a discussion on these validation results from the application perspective will be very useful. Or perhaps the retrievals are only useful to document trends in ammonia and not for real time applications in models?

The AIRS NH₃ current products are at 45 km resolution to recover cloudy pixels, and therefore, increasing global coverage. However, AIRS NH₃ retrievals for single view pixels at 13.5 km resolution are possible for clear-sky only cases. The resolution of 45 km is higher than many global models, and when applied to high resolution localized models, cautions need to be taken so the spatial resolutions are matched. We believe our products provide significant value to the modeling field not only in the trend studies, but also spatial distribution by validation to the modeled properties.

I am also a little concerned that the authors have not compared global maps of ammonia from AIRS to other correlative measurements from other satellites (IASI for example). Although instrument and algorithm differences can exist, readers can look at the comparisons in a qualitative sense and decide for themselves if the product is useful for certain applications or not. Also, for validation results please provide information on the geographic location for each profiles to get a sense on where these observations taken (terrain, surface emissivity, etc.)

We have carried out preliminary comparison with IASI's published results. It is in our plan to carry out detailed quantitative comparison, which should results in a separate manuscript. We added the following sentence to describe the environment of the central valley location where DISCOVER-AQ CA took place: "The in-situ NH₃ vertical profiles were made in the Southern San Joaquin Valley of California. This region inside the central valley of California, between the coastal mountains in the west and the Sierra Nevada Mountains in the east, consists largely of farmland with scattered dairy farms. Although most of the area is rural, the profiles were made near the small cities of Hanford and Corcoran."

The authors presumably are continuing their collaboration with field campaign programs and therefore should recommend to the campaign that future experiments should focus doing multiple spirals within a short distance of each other in a 45-km box to understand sub-grid variability of ammonia.

Great suggestion.

In Figure 4, the color bar is referred to as x-axis.

We have corrected this.

There is a lot of discussion on the relevance of biomass burning and ammonia distribution observed in global maps. I think the authors are correct in drawing those correlations but

would be nice to correlate with MODIS fire activity maps. Without corroboration from other sources of information, it becomes speculative at best. I say this because in Russia and Siberia, there seem to be elevated ammonia in all seasons and number of retrievals (days of data available) low. Could it be that there are some retrieval issues owing to the persistent snow on the ground? Again, this is why it is important to compare AIRS ammonia retrievals with other satellite retrievals to establish biases as a function of season and location. The 2-week time period is not enough to capture the dynamic range, seasonal, and regional variability seen in ammonia to validate the product.

We agree that continued validation and intercomparisons are important and they are in our plans to do. This manuscript aims to introduce the AIRS NH₃ new product and document the algorithm applied. Even though we did not have the space to show the verification of this product with MODIS fire counts as well as correlation with other trace gas species (i.e., carbon monoxide), this has been in our regular practice in the algorithm development stage. Any potential retrieval artifacts were taken care of in the algorithm.

Minor comment: The few sentences dedicated to World Bank data on page 12 can become a footnote to avoid distracting the reader.

We have removed the sentences and added them as a footnote.

Figure 9 is cited twice. Should there be a Figure 10?

There is only Figure 9, and we have made sure they are used in the right content.

In global season maps, African biomass burning appears to show up prominently in MAM season. However this March peak is absent in Figure 9 for SH. Is it masked by the global averaging? Should this analysis be stratified into crop lands, forests etc. to separate agricultural burning vs. wildfires? I think this stratification will gel nicely with the way the results are presented in Figure 6. In summary, this is important work that should be published after addressing the comments above.

We divided the hemispheres at the equator and most of the African fires in MAM located in the NH. To separate agricultural burning vs. wildfires, and to study the land type vs. emissions require in depth study that is beyond the scope of this paper.

We appreciate very much reviewer #3 for believing that this is an important work. More research of this new product is needed from a greater community once the data is distributed upon preliminary validations.

1 **The Global Tropospheric Ammonia Distribution as seen in the 13-year AIRS**
2 **Measurement Record**

3 Warner, J.X.¹, Z. Wei¹, L. L. Strow², R. R. Dickerson¹, J. B. Nowak³

4

5 ¹Department of Atmospheric and Oceanic Science, University of Maryland College Park,
6 College Park, MD 20742, U.S.A.

7 ²Department of Physics and Joint Center for Environmental Technology, University of Maryland
8 Baltimore County, Baltimore, MD 21250, U.S.A.

9 ³Aerodyne Research, Inc., Billerica, MA 01821, U.S.A.

10

11

12

13

14

15

16

17

18

19

20

21

22

23

24

25

26

27

28

29

30

31

32 **Abstract:**

33

34 Ammonia (NH₃) plays an increasingly important role in the global biogeochemical cycle of
35 reactive nitrogen as well as in aerosol formation and climate. We present extensive and nearly
36 continuous global ammonia measurements made by the Atmospheric Infrared Sounder (AIRS)
37 from the Aqua satellite to identify and quantify major persistent and episodic sources as well as
38 to characterize seasonality. We examine the 13-year period from September 2002 through
39 August 2015 with a retrieval algorithm using an optimal estimation technique with a set of three,
40 spatially and temporally uniform a priori profiles. Vertical profiles show good agreement (~5 –
41 15%) between AIRS NH₃ and the in situ profiles from the winter 2013 DISCOVER-AQ field
42 campaign in central California, despite the likely biases due to spatial resolution differences
43 between the two instruments. AIRS captures the strongest consistent NH₃ [concentrations due to](#)
44 emissions from the anthropogenic (agricultural) source regions, such as South Asia
45 (India/Pakistan), China, the US, parts of Europe, Southeast Asia (Thailand/Myanmar/Laos), the central
46 portion of South America, as well as Western and Northern Africa. These correspond primarily
47 to irrigated croplands, [as well as regions with heavy precipitation](#) with extensive animal
48 feeding operations and fertilizer applications where a summer maximum and a secondary spring
49 maximum are reliably observable. In the Southern Hemisphere (SH) regular agricultural fires
50 contribute to a spring maximum. Regions of strong episodic emissions include Russia and
51 Alaska as well as parts of South America, Africa, and Indonesia. Biomass burning, especially
52 wildfires, dominate these episodic NH₃ [high concentrations](#).

53

54

55

56

57

58

59

60

61

62

Juying Warner 4/5/16 12:36 PM
Deleted: emissions

64 **1. Introduction**

65

66 Global ammonia (NH₃) emissions are increasing due to the increased agricultural livestock
67 numbers coupled with the increasing use of nitrogen fertilization (Sutton et al., 2007, 2008).
68 Atmospheric ammonia has impacts upon local scales, acidification and eutrophication of the
69 ecosystems, and international (transboundary), as well as local, scales through formation of fine
70 ammonium containing aerosols. Ammonia reacts rapidly with sulfuric (H₂SO₄), nitric (HNO₃),
71 and hydrochloric (HCl) acids to form a large fraction of secondary aerosols, i.e., fine Particulate
72 Matter (PM_{2.5}) (particles less than 2.5 micrometers in diameter) (Malm et al., 2004). These
73 ammonium containing aerosols affect Earth's radiative balance, both directly by scattering
74 incoming radiation and indirectly by acting as cloud condensation nuclei (e.g., Adams et al.,
75 2001; Martin et al., 2004; Abbatt et al., 2006; Wang et al., 2008; Henze et al., 2012). A large
76 percentage of PM_{2.5} can penetrate human respiratory systems and deposit in the lungs and
77 alveolar regions, thus endangering public health (e.g., Pope et al., 2002). Ammonia deposition
78 [modifies the transport lifetimes, and deposition patterns of sulfur dioxide \(SO₂\) and nitrogen](#)
79 [dioxide \(NO_x\) \(Wang et al., 2008; Henze et al., 2012\). Additionally, ammonia increases the](#)
80 concentrations of the greenhouse gas nitrous oxide (N₂O) (EPA, 2011) and, [together with](#)
81 [NH₄⁺ content in soils, NH₃ is involved in CH₄ production and release \(Fowler et al., 2009\).](#) NH₃
82 can also contribute to increases in radiative forcing through conversion of organic carbon (OC)
83 into brown carbon (BrC) (Updyke et al., 2012). Therefore, monitoring NH₃ global distribution of
84 sources is very important to human health, with respect to air and water quality, and climate
85 change.

86

87 Atmospheric ammonia concentrations have been modeled from a three-dimensional coupled-
88 oxidant-aerosol model (GEOS-Chem) (Bey et al., 2001) to estimate natural and transboundary
89 pollution influences on sulfate-nitrate-ammonium aerosol concentrations in the United States
90 (Park et al., 2004). [We used the simulated NH₃ fields from GEOS-Chem as the retrieval a priori](#)
91 [for this study.](#) A number of ammonia related science studies and top-down inventory studies are
92 based on GEOS-Chem and its adjoint (Henze et al., 2009; Heald et al., 2012; Zhu et al., 2013;
93 Paulot et al., 2013; 2014; Paulot and Jacob, 2014). The model's ammonia emissions were based
94 on annual data from the 1990 1° x 1° GEIA inventory of Bouwman et al. (1997). Table 1b from

Juying Warner 4/7/16 12:26 PM
Deleted: dditionally, a

Juying Warner 4/7/16 12:31 PM
Deleted: methane

Juying Warner 4/7/16 12:31 PM
Deleted: CH₄

Juying Warner 4/7/16 12:27 PM
Deleted: , and

Juying Warner 4/7/16 12:17 PM
Deleted: modifies the transport lifetimes, and deposition patterns of sulfur dioxide (SO₂) and nitrogen dioxide (NO_x).

102 Park et al. (2004) shows a summary of global and contiguous U.S. ammonia emissions for 2001.
103 The inventory's categories include anthropogenic sources: domesticated animals, fertilizers,
104 human bodies, industry, fossil fuels, and natural sources: oceans, crops, soils, and wild animals.
105 Additional emissions from biomass burning and biofuel used were computed using the global
106 inventories of Duncan et al. (2003) and Yevich and Logan (2003), with an emission factor of 1.3
107 g NH₃ per kilogram dry mass burned (Andreae and Merlet, 2001). For the emissions from
108 domesticated animals and soils, the GEOS-Chem model used the exponential dependencies on
109 temperature reported by Aneja et al. (2000) and Roelle and Aneja (2002), respectively. Ammonia
110 emissions from crops and fertilizers were assumed to vary seasonally with the number of
111 daylight hours (Adams et al., 1999). Seasonal variations in biomass burning and biofuel
112 emissions in the model were specified based on satellite observations (Duncan et al., 2003) and
113 the heating degree-days approach (Park et al., 2004). The GEOS-Chem model can be used to
114 generate 3-D global monthly mean fields of NH₃ concentrations, or higher temporal resolution
115 for various years.

116
117 Satellite remote sensing offers unique opportunities to monitor environmental variables with
118 temporal and spatial variability. Ammonia measurements with large, daily global coverage are
119 challenging and lacking, partly due to the relatively short (hours to a day) lifetime of NH₃ near
120 the Earth's surface, and partly because its retrievals require high sensitivity that can be only
121 obtained from areas with high thermal contrast (TC, the temperature difference between that of
122 the surface temperature and of the first discernable atmospheric layer) near the surface (Clarisse
123 et al., 2010). First measurements of ammonia from space were reported over Beijing and San
124 Diego, CA areas with the Tropospheric Emission Spectrometer (TES, Beer et al., 2008) and in
125 biomass burning plumes with the Infrared Atmospheric Sounding Interferometer (IASI, Coheur
126 et al., 2009) satellite. Shephard et al. (2011) documented the TES ammonia retrieval
127 methodology. TES NH₃ data has been utilized jointly with GEOS-Chem in various emission
128 source studies (e.g. Zhu et al., 2013; Walker et al., 2012; Alvarado et al., 2011; Pinder et al.,
129 2011). Luo et al. (2014) compared TES NH₃ versus carbon monoxide (CO) ratios, using data
130 from Park et al. (2007), to those from the GEOS-Chem model with a focus on biomass burning emissions
131 using TES representative volume mixing ratio values (Shephard et al., 2011).

132

Juying Warner 4/5/16 11:51 PM

Deleted: We use these simulated NH₃ fields as the retrieval a priori for this study.

Juying Warner 3/25/16 4:56 PM

Deleted: the

136 The first global map of ammonia was created from IASI measurements by correlating observed
137 brightness temperature difference and NH₃ total columns using averaged datasets from 2008
138 (Clarisse et al., 2009). It was later concluded that this method tends to underestimate the global
139 emission inventories at a number of global NH₃ hotspots using IASI radiances. Clarisse et al.
140 (2010) examined the ammonia amounts in the San Joaquin Valley using an optimal estimation
141 (OE) retrieval method (Rodgers, 2000) with a global uniform a priori and IASI radiances and
142 compared with TES measurements. They studied the factors influencing the ability to use
143 satellite infrared (IR) instruments to retrieve accurate NH₃ columns and concentrations, finding
144 that the main factors were NH₃ concentrations and thermal contrast. They concluded that through
145 retrieval and forward radiative transfer model runs, if both of the NH₃ concentrations and
146 thermal contrast are large enough, it is possible to quantify ammonia near the lowest level of the
147 atmosphere. R'Honi et al. (2013) discussed the elevated concentrations of NH₃ and HCOOH
148 emitted by the 2010 Russian wildfires. Heald et al. (2012) used contributions from IASI
149 ammonia products in the GEOS-Chem study of inorganic aerosol loading and atmospheric
150 ammonia concentrations over the tropics.

152 Global ammonia sources and variability based on continuous monitoring with longer than a
153 decade record (13 years) have not been available. This study introduces a newly developed daily
154 and global ammonia product from the Atmospheric Infrared Sounder (AIRS) on the NASA EOS
155 Aqua satellite hyperspectral measurements spanning September 2002 through August 2015. The
156 AIRS orbit covers nearly the entire globe twice daily, and due to cloud clearing, recovers up to
157 70% of cloudy coverage (Susskind et al., 2003; Warner et al., 2013). Additionally, AIRS is in the
158 afternoon equator crossing time; and therefore, it offers high sensitivity due to higher surface
159 temperature and provides higher thermal contrast to NH₃ measurements.

161 In the next section, we detail the methodology used to develop the global products of NH₃ and
162 present the discussions for data quality. In Section 3, we show examples of validation cases
163 using in situ data from a recent NASA aircraft mission – DISCOVER-AQ (Crawford et al.,
164 2014) (<http://discover-aq.larc.nasa.gov>). Section 4 illustrates the global distributions of the NH₃
165 sources. We demonstrate the seasonal variability of NH₃ concentrations using AIRS 1
166 measurements in Section 5, before summarizing results in Section 6.

Juying Warner 4/6/16 9:16 AM

Deleted: emissions

Juying Warner 4/6/16 9:16 AM

Deleted: in

Juying Warner 4/6/16 9:20 AM

Deleted: longterm (13 years)

Juying Warner 4/6/16 9:21 AM

Deleted: have

Juying Warner 4/5/16 12:51 PM

Deleted: emissions

172

173 **2. Methodology**

174

175 AIRS is a grating spectrometer with 2378 separate spectral channels between 650-2670 cm^{-1}
176 (15.3-3.8 μm) with a spectral resolving power on the order of 1200. Twelve channels of the
177 AIRS radiances in the window regions (860 – 875, 928 – 932, and 965 – 967 cm^{-1}) are currently
178 used to retrieve NH_3 . These channels are carefully selected so that the retrievals are based on the
179 NH_3 sensitivity, while the effects of surface and overlapping gases are minimized. AIRS cloud
180 clearing, described by Susskind et al. (2003), increases the data coverage significantly to nearly
181 50 – 70% of the total measurements, instead of the pure clear coverage of approximately 10 –
182 15% at a 13.5 km^2 single-view pixel size (Warner et al., 2013). AIRS NH_3 retrievals are based on
183 the cloud-cleared radiances (CCRs) from AIRS L2 products. The averaging kernel (AK) peaks at
184 about 918 hPa giving AIRS good sensitivity to lower tropospheric NH_3 because the planetary
185 boundary layer generally extends above this altitude at the overpass local time of 1:30 pm.

186

187 The algorithm used in this AIRS NH_3 study was based on a retrieval module developed for AIRS
188 carbon monoxide (CO) products (Warner et al., 2010). This module was built upon and added to
189 the current AIRS operational system or team algorithm (Susskind et al., 2003), but used a
190 different minimization method. The NH_3 module uses AIRS Version 6 (V6) Level 2 (L2)
191 profiles and errors from the previous retrieval steps (i.e., surface, clouds, water vapor, ozone,
192 methane, CO) as input to the AIRS forward model – the Stand-alone AIRS Radiative Transfer
193 Algorithm (SARTA) (Strow et al., 2003). We used SARTA with the addition of NH_3 as a
194 variable gas, which was carried out by co-author, Strow and [redacted], since the official AIRS
195 forward model does not include NH_3 absorption as a variable. AIRS NH_3 retrievals use an OE
196 method following the formulations given by Rodgers (2000), and also described by Pan et al.,
197 (1998). The OE retrieval output quantities not only include the NH_3 concentrations, but also
198 provide the AKs, the error covariance, and the degrees of freedom for signal (DOFS), which
199 benefit model verifications and data assimilation by using well-quantified errors.

200

201 Given a model of the instrument's signals, in the OE method, the forward equation for the NH_3
202 profile retrieval problem can be written as:

Juying Warner 3/25/16 4:40 PM

Deleted: s

Juying Warner 3/25/16 4:40 PM

Deleted: Hannon

205

$$206 \quad \mathbf{y} = \mathbf{f}(\mathbf{x}, \mathbf{b}) + \mathbf{n}, \quad (1)$$

207

208 where \mathbf{y} is the vector of measured radiances, \mathbf{x} is the state vector (variables to be retrieved from
209 the measurements), \mathbf{b} represents all other parameters used by the forward model, $\mathbf{f}(\mathbf{x}, \mathbf{b})$ is the
210 forward model function, and \mathbf{n} is the instrument noise. For the variables that obey a Gaussian
211 distribution, this inverse problem is equivalent to the maximum likelihood solution. By using a
212 Newtonian iteration; the solution to equation (1) can be written as (Rodgers, 2000):

213

$$214 \quad \mathbf{X}_{n+1} = \mathbf{x}_a + \mathbf{C}_a \mathbf{K}_n^T (\mathbf{K}_n \mathbf{C}_a \mathbf{K}_n^T + \mathbf{C}_e)^{-1} [\mathbf{y} - \mathbf{y}_n - \mathbf{K}_n (\mathbf{x}_a - \mathbf{x}_n)] \quad (2)$$

215

216 where n is the order of iteration and \mathbf{C}_e is the measurement error covariance matrix.

217 $\mathbf{K}_n = \partial \mathbf{f}(\mathbf{x}, \mathbf{b}) / \partial \mathbf{x}$ is the jacobian matrix for iteration n , which is the sensitivity matrix of the
218 forward model to the state vector \mathbf{x} . \mathbf{x}_a is the mean of the a priori distribution and \mathbf{C}_a is the a
219 priori error covariance matrix for \mathbf{x}_a .

220

221 As defined by the retrieval formulations, the AKs are computed using the following:

222

$$223 \quad \mathbf{A} = \mathbf{C}_a \mathbf{K}^T (\mathbf{K} \mathbf{C}_a \mathbf{K}^T + \mathbf{C}_e)^{-1} \mathbf{K} \quad (3)$$

224

225 and,

226



$$227 \quad \mathbf{x}' \approx \mathbf{A} \mathbf{x} + (\mathbf{I} - \mathbf{A}) \mathbf{x}_a, \quad (4)$$






228

229 where \mathbf{I} represents the identity matrix and \mathbf{x} is the true state. Equation (4) states that in the
230 absence of other error sources the retrieved state is a weighted mean of the true state and the a
231 priori state, with the weight \mathbf{A} for the true state and $\mathbf{I} - \mathbf{A}$ for the a priori. This shows the
232 importance of AKs as diagnostics of the retrieval. The closer the matrix \mathbf{A} is to the identity
233 matrix the more the retrieved state resembles the true state.

234

235 The optimal estimation method requires an a priori mean profile and a corresponding error

236 covariance matrix that represent the current knowledge of the geophysical property, i.e., NH₃,
237 prior to the retrieval. Due to the high spatial variability and short lifetime of NH₃, a simple fixed
238 a priori for all emission scenarios is not appropriate. We developed a global mean, multi-year
239 averaged (2003-2012), three-tier a priori from GEOS-Chem model (v9-02) simulations for high,
240 moderate, and low [pollutions](#). We used GEOS-5 MERRA datasets from the NASA Global
241 Modeling and Assimilation Office (Rienecker et al., 2011) to drive the meteorological fields in
242 the GEOS-Chem simulations. Figure 1 shows the a priori mean profiles (solid curve with
243 squares) and the error covariance matrices (horizontal bars) for the low (left panel), the moderate
244 (middle panel), and the high [pollution](#) (right panel), respectively. The high [pollution](#) range was
245 defined by profiles with Volume Mixing Ratios (VMRs) greater than or equal to 5 parts-per-
246 billion-volume (ppbv)  surface. The moderate [pollution](#) range includes the profiles with surface
247 VMRs greater than or equal to 1 ppbv but less than 5 ppbv, or greater than 1 ppbv at any level
248 between the surface and 500hPa. The low [pollution](#) is then defined as being lower than the lower
249 bounds of the moderate [pollution](#) range. The profiles were adjusted to match AIRS forward
250 model levels. The modeled profiles are extrapolated near the surface with additional constraints
251 to reflect values that are likely seen by satellite sensors. 

252
253 Although for  a pixel there are three possible a priori  the same set of the three-tier a priori 
254 used globally and throughout the AIRS data record. Thus, any spatial and temporal NH₃
255 variations detected using this algorithm are from AIRS measurements. To select one of the three
256 a priori  for each AIRS pixel, we examine the brightness temperature difference between a strong
257 and a weak channel, divided by the measurement noise of the strong channel, defined as a
258 “difference of brightness temperature index” (DBTI). This is similar to the method used by TES
259 NH₃ and described by Shephard et al. (2011). The DBTIs vary with meteorological conditions
260 and, most importantly, the thermal contrast at the surface. To take into account of these effects,
261 we simulate the relationship between the brightness temperature differences and TC under
262 various meteorological conditions using SARTA. We randomly picked 13790 profiles from
263 AIRS L2 products over land from the months of January, April, July, and October in years 2003,
264 2008, and 2011. We then perturbed the NH₃ values spanning the three a priori mean profiles
265 using the range of 0 – 100 ppt  each atmospheric profile. The observed brightness
266 temperatures are compared with the simulated values at a given TC to determine the level of a

Juying Warner 4/5/16 12:58 PM
Deleted: level

Juying Warner 4/5/16 1:00 PM
Deleted: emission levels

Juying Warner 4/5/16 2:18 PM
Deleted: emission

Juying Warner 4/5/16 2:18 PM
Deleted: emission

Juying Warner 4/5/16 2:18 PM
Deleted: emission **levels**

Juying Warner 4/5/16 1:01 PM
Deleted: emission

Juying Warner 4/5/16 1:01 PM
Deleted: emission

Juying Warner 4/5/16 1:02 PM
Deleted: levels

Juying Warner 4/5/16 1:02 PM
Deleted: level

276 priori for the full retrievals. Figure 2 depicts a relationship between the DBTI and DOFS for the
277 three emission levels with low emissions in blue, moderate emissions in green, and high
278 emissions in red. The higher DBTIs are correlated with higher DOFS, which represent higher
279 surface thermal contrast (Deeter et al., 2007).

280

281 The NH₃ retrieval quality assurance levels are determined based on the retrieval sensitivities
282 under various meteorological and surface conditions using the AKs and the DOFS. We also take
283 into account the performance of the retrievals against surface thermal contrasts from AIRS
284 products. Additionally, we examine the retrieval residuals, χ^2 , and the number of iterations to set
285 proper quality assurance flags. The NH₃ retrieval quality is affected by the meteorological
286 properties, such as the vertical temperature and water vapor profiles, surface temperatures, and
287 emissivity, which are used to model the atmosphere. We also adapt the error information

288 provided by the AIRS CCR for the relevant channels, which includes meteorological quantities
289 that are used in deriving the AIRS CCR
290 (http://disc.sci.gsfc.nasa.gov/AIRS/documentation/v6_docs/v6releasedocs1/V6_Level_2_Cloud_Cleared_Radiances.pdf). This error information is flagged by Q0, Q1, and Q2 with Q0 having
291 the highest quality and Q2 being unusable. In the remaining discussions of this study, we used χ^2
292 between 0.9 and 27, considering that the channels used are not all spectrally independent. The
293 number of iterations limit was set at 10, meanwhile, only the cases with retrieval residuals less
294 than 1 K are used. We also excluded cases with the surface thermal contrast between -4 and +4 K,
295 to avoid ambiguous a priori levels; however, this primarily affects areas over the global oceans.
296 Any additional screening of the data for higher quality requirements, the use of DOFS, will
297 be discussed case by case. Although we have developed AIRS NH₃ products for all available
298 datasets, only the daytime and land cases are discussed in this study. Additionally, only radiances
299 with quality flag as Q0 are selected for the discussions in the following sections to ensure the
300 best accuracy.

301

302 **3. Validation with in situ measurements**

303

304 Validations of retrievals using in situ measurements are vital to quantifying uncertainties in the
305 concentrations, sources, transport patterns, and trends using satellite data. Direct measurements
306

Juying Warner 4/5/16 1:06 PM

Deleted: emissivity, that

308 of tropospheric NH₃ are relatively sparse and in situ measurements above the ground level,
309 necessary to validate satellite retrievals, are available for only limited locations and time periods
310 (e.g. Nowak et al., 2007, 2010, and 2012). Validation of AIRS NH₃ datasets with available in
311 situ measurements is a continuous effort as more in situ measurements become available. As an
312 example of our validation effort, we use the DISCOVER-AQ NH₃ measurements over California
313 (<https://www-air.larc.nasa.gov/cgi-bin/ArcView/discover-aq.ca-2013-->). The sampling inlet and
314 NH₃ calibration set-up used during DISCOVER AQ with the cavity ring down spectrometer
315 (CRDS) (G2103, Picarro Inc.) is the same as used with the Chemical Ionization Mass
316 Spectrometry (CIMS) and described in Nowak et al. (2007). The CRDS, aboard the NASA P-3B
317 aircraft during DISCOVER-AQ CA, data period covers January 16 to February 06, 2013. [The in-](#)
318 [situ NH3 vertical profiles were made in the Southern San Joaquin Valley of California. This](#)
319 [region inside the central valley of California, between the coastal mountains in the west and the](#)
320 [Sierra Nevada Mountains in the east, consists largely of farmland with scattered dairy](#)
321 [farms. Although most of the area is rural, the profiles were made near the small cities of Hanford](#)
322 [and Corcoran.](#) We only select spiral profiles from the flights within 45 km of the center of the
323 retrieved AIRS profiles, for the closest match, and within 3 hours of the measurement window,
324 similar to the method used for AIRS CO validation (Warner et al., 2006).

325
326 Figure 3 shows four retrieval profiles that show high NH₃ concentrations and meet the matching
327 criteria, where the red curves represent AIRS retrieved profiles, gray curves are the a priori
328 profiles, green solid lines are in situ spiral profiles, and the blue dashed lines are the convolved
329 in situ profiles by AIRS NH₃ AKs. Note that in Fig. 3, the x-axis is linear from 0 to 25 ppbv and
330 logarithmic from 25 to 150 ppbv. The convolved in situ profiles take into account satellite
331 retrieval sensitivities, making them appropriate to compare against satellite retrievals (Re
332 and Connor, 2003). The convolution calculations follow Eq. (3) and (4) in Sec. 2. The top left
333 panel shows a case measured on January 16, 2013 with the retrieval quality at 0, DOFS at 0.64,
334 χ^2 at 1.91, the retrieval residual at 0 and the measurement time differences at 1.31 hours. The
335 distance between the in situ profile and the center of the AIRS profile is approximately 13.5 km.
336 The top right panel shows four in situ profiles from January 21, 2013 with AIRS retrieved profile
337 quality at 0, DOFS at 0.66, χ^2 at 1.26, the retrieval residual at 0.07, the time differences ranging
338 from 0.58 to 1.68 hours, and the distance differences at approximately 56 km for all four profiles.

Juying Warner 4/5/16 7:06 PM
Deleted: green

340 The two profiles in the bottom left panel are also from January 21, 2013, with quality at 0, DOFS
341 at 0.83, χ^2 at 0.31, the retrieval residual at 0.06. The time differences to the AIRS retrieved
342 profile are 1.02 and -1.25 hours, and the distances are 38.3 and 38.7 km, respectively. In the
343 bottom right panel, there are four profiles taken from February 4, 2013, with the retrieval profile
344 quality at 0, DOFS at 0.84, χ^2 at 1.1, and the retrieval residual at 0.05. The time differences
345 between the in situ and the retrieved profiles are 1.63, 1.40, -0.47, and -0.71, and the distances
346 are 5.1, 45.2, 4.9, and 45.2 km, respectively. Some of the AIRS retrievals collocate with several
347 in situ profiles, and these show substantial spatial variability.


348


349 Over regions with high NH_3 in situ concentrations, the convolved in situ profiles agree with the
350 retrievals within <1 to ~3 ppbv (~5-15%) near the top of the boundary layer, as seen in the top
351 two panels in Fig. 3. These two AIRS NH_3 profiles show good retrieval sensitivities with DOFS
352 at approximately 0.64 and 0.66, χ^2 at 1.91 and 1.26, and the residual at 0.07, respectively. The
353 top left in situ profile is relatively close (13.5 km) to the center of the AIRS pixel, whereas the
354 top right in situ profiles are further away (~46 km) from the center of the AIRS pixel. When the
355 NH_3 amount is low and there is very little sensitivity in AIRS measurements, the convolved
356 profiles converge to the a priori profiles, as seen in the profiles with low NH_3 concentrations in
357 the top right panel and in the bottom left panel. In the bottom right panel, there are four in situ
358 profiles close to the AIRS profile – the AIRS pixel measures the average effect of the area
359 represented by the four in situ profiles. Below 925 – 950 hPa in height, the in situ NH_3 mixing
360 ratios are significantly higher than the retrieved profiles, indicating a limitation of satellite
361 remote sensing in capturing near surface composition properties. Note again that each AIRS
362 profile covers a surface area of 45 km² where in situ observed NH_3 amounts can vary by a factor
363 of ten. The aircraft in situ flights sometimes are biased by their proximity to strong local point
364 sources. Therefore, the differences between the retrievals and in situ measurements are likely due
365 to sampling issues, although the retrieved profile matches the average of the in situ profiles as
366 discussed above. [Nonetheless, the vertical profiles show good agreement \(~5 – 15%\) between
367 AIRS \$\text{NH}_3\$ and the in situ profiles in the examples given above.](#)

368

369 **4. Global Ammonia Concentrations**

370

371 The AIRS global NH₃ VMRs at 918 hPa, averaged from  2002 through Aug. 2015, are
372 shown in the upper panel of Fig. 4. The lower panel in Fig. 4 shows the total occurrences of
373 elevated emissions (VMRs \geq 1.0 ppbv at 918 hPa) for the same dataset. The occurrences, in
374 numbers of days, are good indicators of the types of emission sources either due to recurring
375 agricultural practices or episodic forest fires. It is important to analyze the NH₃ VMRs together
376 with the occurrences to identify major emission sources. Another important quantity used in the
377 NH₃ source analysis is the retrieval DOFS. Figure 5 shows the AIRS NH₃ DOFS values being in
378 a range of 0.1 to slightly above 1.0. The regions with DOFS greater than 0.4 are generally
379 associated with high NH₃ emissions and strong signal to noise ratios. We used a threshold level
380 of DOFS of 0.1 to screen the retrievals in the Fig. 4 top panel to eliminate noise and to focus on
381 where AIRS sensitivity is high. Areas with DOFS $<$ 0.1 in the whole data record are indicated in
382 white. The AIRS retrievals are sensitive to NH₃ concentrations in the lowest layer of the
383 atmosphere between 850 hPa and the surface, with sensitivity peaking at approximately 918 hPa
384 based on the retrieved AKs (not shown). Therefore, we use NH₃ VMRs at this level for all
385 discussions in this study. There are diurnal variations in the datasets (not shown) that may be due
386 to a number of factors including the day-night differences of emissions and chemical reactions
387 and possibly measurement sensitivities, which is beyond the scope of this paper and will be
388 studied at a later time. Also note that the missing data over land in certain regions are either due
389 to high elevation (above the 918 hPa altitude level), and therefore not shown, or persistent
390 cloudy days.

391
392 Globally, AIRS shows strong NH₃ [hotspots](#) from biogenic and anthropogenic sources including
393 South Asia (India/Pakistan), East Asia (China), the central U.S., parts of Europe, Southeast Asia
394 (Thailand/Myanmar/Laos), the central portion of South America, and Western and Northern
395 Africa, where both the NH₃ VMRs and the frequent occurrences are high. The primary sources
396 for these regions are from human activities, e.g., livestock waste management and other
397 agricultural activities. The NH₃ concentrations over these hot spots vary from ~2.5 to above 10
398 ppbv, averaged over 13 years covering both strong and weak emission periods. Also seen are
399 large regions of high NH₃ concentrations due to biomass burning events over Russia, Alaska,
400 South America, Africa, and Indonesia, represented by high VMRs and low frequer  High
401 concentrations of NH₃ are persistent over South America and reflect emissions from biomass

Juying Warner 4/5/16 11:23 PM

Deleted: emissions

403 burning that are trapped by the Andes
404 http://earthobservatory.nasa.gov/IOTD/view.php?id=8033&eocn=image&eoci=related_image.
405 The hot spot over South Asia corresponds to the heavily populated Indo-Gangetic Plain with
406 plentiful, fertile croplands and extensive livestock, and bounded on the north by the Himalayas
407 (Yamaji et al., 2004). The absolute maximum on Fig. 4 is found over the Punjab which has the
408 highest population density in Pakistan.
409
410 To understand the persistent emission sources, we filtered the NH₃ VMRs with the collocated
411 occurrences of elevated emissions (≥ 1.4 ppbv) using a threshold of 40 days and the results are
412 shown in Fig. 6 top panel. Although a sufficient emission (≥ 1.4 ppbv) threshold is used to
413 calculate occurrences of the persistent sources, we used all VMR values, with DOFS greater than
414 0.1, for the VMR maps. The persistent NH₃ sources not only include those large regions listed
415 above, but also include small geographical areas such as in the San Joaquin Valley of central
416 California in the U.S. (with low sulfur emissions and where livestock are plentiful); the Po
417 Valley, Italy; Fergana Valley, Uzbekistan; Azerbaijan; the Nile Delta and along the banks of the
418 Nile River in Egypt; and the Sichuan Basin in China. Some of these source locations are
419 consistent with those previously reported by Clarisse et al. (2009). These emission hotspots are
420 compared with the “Pasture and Cropland Map” (see middle panel in Fig. 6), posted by
421 <http://OurWorldInData.org>, located at the Institute for New Economic Thinking at the Oxford
422 Martin School. AIRS NH₃ source regions are strongly correlated with cropland areas, e.g., over
423 India, China, the middle U.S., Western Africa, eastern South America, and Europe. Note that
424 four of the strongest emission regions correspond to high percentage irrigated agricultural areas
425 (see bottom panel in Fig. 6), i.e., over Pakistan, India, northern Italy, and Azerbaijan adjacent to
426 the Caspian Sea. The irrigated agricultural land includes that irrigated by controlled flooding.
427 These data are provided by the World Bank (data.worldbank.org), where the color values are the
428 percent agricultural irrigated land of total agricultural land. These irrigation activities are
429 associated with periods of fertilization and ammonia release. Sommer et al. (2004) studied the
430 relationship between the fertilizing time and the ammonia release time and indicated that the
431 fertilizers applied in March can be released in the June to August time frame depending on the
432 amount of precipitation. The irrigation practices may have the same effect as high amounts of
433 precipitation.

Juying Warner 4/7/16 7:21 PM

Deleted: with a statement that the maps displayed on the World Bank web site are for reference only and do not imply any judgment on the legal status of any territory, or any endorsement or acceptance of such boundaries

Juying Warner 4/7/16 7:22 PM

Deleted: . T

440

441 Over China, the AIRS retrieval can match high-resolution inventories distinguishing the two
442 major animal husbandry areas in east-central China (Henan, Shandong, and Hebei provinces) as
443 well as Sichuan to their southwest (Huang et al., 2012). Additional weaker, but persistent, NH₃
444 sources are also seen in the Fig. 6 top panel that are likely related to livestock and agriculture
445 practices. These source regions include areas in eastern North Carolina (consistent with Wu et al.,
446 2008), Arizona near Phoenix, in the east coast of Spain near Barcelona and Águilas, and over
447 large areas in the Netherlands, in Mozambique in Africa, and the Gambela National Park region
448 between Ethiopia and South Sudan.

449

450 5. Seasonal Variability

451

452 Seasonal variations are shown in Fig. 7 in the four NH₃ VMR maps, averaged between Sept.
453 2002 and Aug. 2015, for December-January-February (DJF, upper left panel), March-April-May
454 (MAM, upper right panel), June-July-August (JJA, lower left panel), and September-October-
455 November (SON, lower right panel), respectively, with DOFS greater than 0.1 and no cutoff for
456 the VMRs. Globally, the strongest emissions are in the NH summer and spring seasons, with the
457 exception from strong biomass burning (BB) sources, i.e., over South America, the Southeast
458 Asia, and Russia in the NH fall season. The highest NH₃ concentrations over non-BB dominant
459 regions occur over India, China, the Mid-West U.S., and part of Europe in the summer months.
460 The longest high emission seasons are over northern India, collocated with the measurement of
461 high NH₄⁺ in the precipitation over India reported by Kulshrestha et al. (2005). The seasonal
462 NH₃ VMR distributions in China, Europe, and the U.S. are also consistent a large extent, with
463 the Paulot et al. (2014) study of agricultural emissions inventory derived by high-resolution
464 inversion of ammonium wet deposition data. This is especially true for the spring season, as seen
465 in Fig. A1 of Paulot et al. (2014), i.e. ASAGE_NH3 (Magnitude and Seasonality of
466 Agricultural Emissions for NH₃, <https://fpaulot.bitbucket.org/MASAGE/>) emissions of NH₃ from
467 fertilizers.

468

469 High average concentrations (Fig. 7) with low frequency (Fig. 8) generally indicate NH₃ from
470 biomass burning (BB). The greatest emissions from BB in the NH appear in the summer months

471 over Siberia and eastern Russia as well as over Alaska, U.S. The highest emissions due to BB in
472 the SH appear over South America in September to November (spring for the SH) when
473 precipitation is minimal and burning extensive (Oliveras et al., 2014). Over SE Asia where the
474 dry season and most BB occurs in March to May, we find another local maximum (Lin et al.,
475 2013). Over Africa high emissions from BB occur in the Western and Central regions, although
476 both high concentrations and frequent fires appear in the Sahel just south of the Sahara in the NH
477 winter. In that region persistent burning of agricultural waste has been reported (Haywood et al.,
478 2008); see also <http://rapidfire.sci.gsfc.nasa.gov/cgi-bin/imagery/firemaps.cgi>.

479
480 Ammonia seasonal variations are presented (Fig. 9) using the monthly mean VMRs averaged
481 over the 13-year period. Simple hemispheric averages of NH_3 concentrations for all cases do not
482 accurately reflect the seasonality of the important agricultural activities in the NH, due to the
483 mixing with BB cases and low NH_3 regions, as well as regions with missing values due to weeks
484 of persistent cloud cover. To understand how NH_3 emissions vary seasonally due to human
485 activities, we focus on the NH_3 emissions from the continuous emission sources. As in the case
486 of Fig. 6, where we showed continuous sources using screening by the occurrences of elevated
487 emissions, we select the occurrence thresholds at emission levels higher than 1.4 ppbv on at least
488 40 days of the 13-year record. Figure 9 shows the monthly mean variations of NH_3 (solid line) in
489 both the NH (upper panel) and the SH (lower panel); the dashed lines show the $\pm 1\sigma$ (standard
490 deviation, STD) and the shaded areas represent the maximum and minimum range of each
491 dataset. In the NH, the high emission period starts in April and the NH_3 concentrations peak in
492 June. The NH average of the VMR concentrations from April through July is in the range of 3.7
493 – 4.0 ppbv; and it gradually decreases to the minimum of below 2 ppbv in November-December-
494 January. The range of monthly mean variability between different years is also larger from April
495 to September (at ~ 1 ppbv) than in the winter months (at ~ 0.4 ppbv). The STD decreases from the
496 summer values of 0.6 ppbv to 0.3 ppbv in the winter.

497
498 Seasonal variation in the SH (lower panel in Fig. 9) shows that the primary sources of NH_3
499 emission are from BB, as was seen in the NH_3 seasonal maps (e.g., Fig. 7). Although the filtering
500 for the continuous emission sources eliminated some large occasional fires (i.e., over Indonesia),
501 there are still regularly occurring fires, such as those over the central part of South America. The

502 NH₃ emission in the SH peaks in September with an average value near 3.5 ppbv and decreases
503 sharply after the SH spring season. The season of high emission in the SH is much shorter than
504 in the NH, as demonstrated by the widths of the seasonal distribution curves. The largest STD
505 occurs in September with a magnitude of 2 ppbv, but the variation between different years in the
506 winter is very small (~0.25 ppbv).

507

508 6. Summary


509

510 Satellite ammonia (NH₃) products with a 13-year data record provide global daily maps, identify
511 major source regions, and show seasonal cycles. This enables studies for detailed locations of the
512 sources and their spatial and temporal variations. AIRS NH₃ products using OE retrievals
513 provide retrieval sensitivity properties, in addition to NH₃ concentrations, such as: the error
514 covariance matrices, and the DOFS. This will facilitate sensor inter-comparisons, model
515 verifications, and data assimilation of satellite retrievals. AIRS measurements can not only
516 capture high biomass burning emissions (e.g., over Russia, Alaska, South America, Africa, and
517 Indonesia) and/or accumulated concentrations such as in various valleys (e.g., San Joaquin
518 Valley, California in the U.S., the Po Valley, Italy, Fergana Valley, Uzbekistan, and the Sichuan
519 Basin in China), but also emissions due to routine animal feeding and agriculture activities (e.g.,
520 Azerbaijan, Nile Delta and along the banks of the Nile River in Egypt, the Mid-West U.S., North
521 Carolina, U.S., the east coast of Spain, in the Netherlands, in Mozambique and Ethiopia, Africa,
522 and especially the Indo-Gangetic Plain of South Asia). Over China, the AIRS retrieval can match
523 high-resolution inventories distinguishing the two major animal husbandry areas in east-central
524 China and the Sichuan Basin. Preliminary validation results show excellent agreement with in
525 situ airborne measurements (to within 5-15% of the retrieved profiles). Note that since each
526 AIRS profile covers a surface area of 45 km² where the NH₃ amounts can vary largely, the
527 simple numerical differences may not be the optimal way to validate satellite ammonia products.

528

529 We use frequent occurrences of NH₃ elevated emissions to select persistent sources. This
530 distinguishes the NH₃ emissions due to human activities versus occasional fires or retrieval noise.

531 We show the persistent ammonia sources correlate well with cropland usage, particularly in
532 regions where irrigation is a routine practice. We show the hemispheric seasonal variation

533 using sources screened by the high NH₃ frequent occurrences. The NH high NH₃ emissions
534 occur in the spring and summer with highest from April to July and lowest in November through
535 January. In the SH, the NH₃ emission is highest in September, this is most likely due to BB
536 emissions shown by the high VRMs and relatively low frequency 

537
538 Detailed examinations of specific regions are needed and will be included in future studies to
539 improve our understanding of the processes that control the NH₃ distribution and variability. The
540 recent NH₃ trends from AIRS 13-year measurements will also be a subject of future studies since
541 the scope of this paper is to focus on the algorithm details and the global distributions. Results in
542 this study are focused on land and daytime only. Future studies will include more complicated
543 surface types, i.e., ocean surfaces and regions with lower thermal contrast. The diurnal variations
544 will also be an important topic in the future studies. We have used the pixels with the highest
545 quality cloud-cleared radiances (at 45 km² spatial resolution) defined by the earlier steps of AIRS
546 retrievals, while a future direction will be to also use the higher spatial resolution single-view
547 pixels (at 13.5 km²) under clear-sky conditions (Warner et al., 2013).

548
549 **Acknowledgement:**

550
551 This study was funded by NASA's The Science of Terra and Aqua program under grant numbers
552 NNX11AG39G and NNX12AJ05G. We wish to acknowledge the GEOS-Chem team, AIRS
553 science team, DISCOVER-AQ team. MERRA data used in this study/project have been provided
554 by GMAO at NASA Goddard Space Flight Center through the NASA GES DISC online archive.
555 [Resources supporting this work were provided by the NASA High-End Computing \(HEC\)](#)
556 [Program through the NASA Center for Climate Simulation \(NCCS\) at Goddard Space Flight](#)
557 [Center.](#)

558
559 **Reference:**

560
561 Abbatt, J. P. D., Benz, S., Cziczo, D.J., Kanji, Z., Lohmann, U., Mohler, O.: Solid Ammonium
562 Sulphate Aerosols as Ice Nuclei: A Pathway for Cirrus Cloud Formation, *Science*, 313, 1770
563 doi:10.1126/science.1129726, 2006.

564 Adams, P. J., Seinfeld, J. H., Koch, D., Mickley, L. and Jacob, D.: General circulation model
565 assessment of direct radiative forcing by the sulfate-nitrate-ammonium- water inorganic
566 aerosol system, *J. Geophys. Res. Atmos.*, 106(D1), 1097–1111, doi: 10.1029/2000JD900512,
567 2001.

568 Adon, M, C. Galy-Lacaux, V. Yoboué, C. Delon, J. P. Lacaux, P. Castera, E. Gardrat, J. Pienaar,
569 H. Al Ourabi, D. Laouali, B. Diop, L. Sigha-Nkamdjou, A. Akpo, J. P. Tathy, F. Lavenu, and
570 E. Mougín: Long term measurements of sulfur dioxide, nitrogen dioxide, ammonia, nitric
571 acid and ozone in Africa using passive samplers, *Atmos. Chem. Phys. Discuss.*, 10, 4407-
572 4461, 2010.

573 Alvarado, M. J., Cady-Pereira, K. E., Xiao, Y., Millet, D. B. and Payne, V. H.: Emission Ratios
574 for Ammonia and Formic Acid and Observations of Peroxy Acetyl Nitrate (PAN) and
575 Ethylene in Biomass Burning Smoke as Seen by the Tropospheric Emission Spectrometer
576 (TES), *Atmosphere* 2(4), 633 – 654, doi:[10.3390/atmos2040633](https://doi.org/10.3390/atmos2040633), 2011

577 Andreae, M. O., and Merlet, P.: Emissions of trace gases and aerosols from biomass burning,
578 *Global Biogeochem. Cycles*, 15, 955 – 966, 2001.

579 Aneja, V. P., Chauhan, J. P. and Walker, J. T.: Characterization of atmospheric ammonia
580 emissions from swine waste storage and treatment lagoons, *J. Geophys. Res.*, 105(D9),
581 11,535–11,545, 2000.

582 Beer, R., Shephard, M. W., Kulawik, S. S., Clough, S. A., Eldering, A., Bowman, K. W., Sander,
583 S. P., Fisher, B. M., Payne, V. H., Luo, M., Osterman, G. B., and Worden, J. R.: First
584 satellite observations of lower tropospheric ammonia and methanol, *Geophys. Res. Lett.*, 35,
585 L09801, doi:10.1029/2008GL033642, 2008.

586 Bey, L., Jacob, D. J., Yantosca, R. M., Logan, J. A., Field, B., Fiore, A. M., Li, Q., Liu, H.,
587 Mickley, L. J., and Schultz, M.: Global modeling of tropospheric chemistry with assimilated
588 meteorology: Model description and evaluation, *J. Geophys. Res.*, 106(D19), 23,073-23,096,
589 2001.

590 Bouwman, A. F., Lee, D. S., Asman, W. A. H., Dentener, F. J., VanderHoek, K. W. and Olivier J.
591 G. J.: A global high-resolution emission inventory for ammonia, *Global Biogeochem. Cycles*,
592 11(4), 561–587, doi:10.1029/97GB02266, 1997.

593 Clarisse, L., Clerbaux, C., Dentener, F., Hurtmans, D. and Coheur, P.-F.: Global ammonia
594 distribution derived from infrared satellite observations, *Nat. Geosci.*, 2, 479-483,
595 doi:10.1038/ngeo551, 2009.

596 Clarisse, L., Shephard, M. W., Dentener, F., Hurtmans, D., Cady-Pereira, K., Karagulian, F.,
597 Damme, M. V., Clerbaux, C. and Coheur P.-F.: Satellite monitoring of ammonia: A case
598 study of the San Joaquin Valley, *J. Geophys. Res.*, 115(D13), 16,
599 doi:10.1029/2009JD013291, 2010.

600 Coheur, P.-F., Clarisse, L., Turquety, S., Hurtmans, D. and Clerbaux, C.: IASI measurements of
601 reactive trace species in biomass burning plumes, *Atmos. Chem. Phys.*, 9, 5655–5667.2009,
602 2009.

603 Crawford, J. H., Dickerson, R. R. and Hains, J. C.: DISCOVER-AQ: Observations and early
604 results, *Environ. Manag.*, September, 2014.

605 Deeter, M. N., Edwards, D. P., Gille, J. C., and Drummond, J. R.: Sensitivity of MOPITT
606 observations to carbon monoxide in the lower troposphere, *J. Geophys. Res.*, 112, D24306,
607 doi:10.1029/2007JD008929, 2007.

608 Dentener, F. J. and Crutzen, P. J.: A three-dimensional model of the global ammonia cycle, *J.*
609 *Atmos. Chem.*, 19, 331-369, 1994

610 Duncan, B. N., Martin, R. V., Staudt, A. C., Yevich, R., and Logan, J. A.: Interannual and
611 seasonal variability of biomass burning emissions constrained by satellite observations, *J.*
612 *Geophys. Res.*, 108(D2), 4100, doi:10.1029/2002JD002378, 2003.

613 [EPA, 2011, Reactive Nitrogen in the United States, A Report to the EPA Science Advisory](#)
614 [Board, 164 pp. 2011.](#)
615 [http://yosemite.epa.gov/sab/sabproduct.nsf/02ad90b136fc21ef85256eba00436459/c83c30afa](http://yosemite.epa.gov/sab/sabproduct.nsf/02ad90b136fc21ef85256eba00436459/c83c30afa4656bea85256ea10047e1e1!OpenDocument&TableRow=2.2)
616 [4656bea85256ea10047e1e1!OpenDocument&TableRow=2.2](http://yosemite.epa.gov/sab/sabproduct.nsf/02ad90b136fc21ef85256eba00436459/c83c30afa4656bea85256ea10047e1e1!OpenDocument&TableRow=2.2)

617 Erisman, J. W., Galloway, J.N., Seitzinger, S., Bleeker, A., Dise, N. B., Petrescu, R., Leach,
618 A.M. and de Vries, W.: Consequences of human modification of the global nitrogen cycle,
619 *Philosophical Transactions of the Royal Society B-Biological Sciences*, 368(1621).
620 DOI: 10.1098/rstb.2013.0116, 2013.

621 [Fowler D., Pilegaard, K., Sutton, M. A., et al., 2009, Atmospheric composition change:](#)
622 [Ecosystems-Atmosphere interactions, ATMOSPHERIC ENVIRONMENT Volume:](#)
623 [43 Issue: 33 Special Issue: SI Pages: 5193-5267.](#)

624 Fowler D., Coyle, M., Skiba, U., Sutton, M. A., Cape, J. N., Reis, S., Sheppard, L. J.,
625 Jenkins, A., Grizzetti, B., Galloway, J. N., Vitousek, P., Leach, A., Bouwman, A. F., Bahl, K.
626 B., Dentener, F., Stevenson, D., Amann, M., Voss, M.: The global nitrogen cycle in the
627 twenty-first century, *Philosophical Transactions of the Royal Society B-Biological Sciences*,
628 368(1621), 2013.

629 Galloway, J. N., Townsend, A. R., Erisman, J. W., Bekunda, M., Cai, Z., Freney, J.R., Martinelli,
630 L.A., Seitzinger, S.P., Sutton, M.A.: Transformation of the nitrogen cycle: Recent trends,
631 questions, and potential solutions, *Science*, 320(5878), 889-892, 2008.

632 Haywood, J. M., Pelon, J., Formenti, P., Bharmal, N.A., Brooks, M.E., Capes, G., Chazette, P.,
633 Chou, C., Christopher, S.A., Coe, H.: Overview of the Dust and Biomass-burning
634 Experiment and African Monsoon Multidisciplinary Analysis Special Observing Period-0, *J.*
635 *Geophys. Res.*, 113, no. 23, DOI:10.1029/2008JD010077, 2008.

636 Heald, C. L., Collett, J. L., Lee, T., Benedict, K. B., Schwandner, F. M., Li, Y., Clarisse, L.,
637 Hurtmans, D. R., Van Damme, M., Clerbaux, C., Coheur, P.-F. and Pye H. O. T.:
638 Atmospheric ammonia and particulate inorganic nitrogen over the united states, *Atmos.*
639 *Chem. Phys.*, 12(21), 10,2 95–10, 312, 2012.

640 Henze, D. K., Hakami, A., Seinfeld, J. H.: Development of the adjoint of GEOS-Chem. *Atmos.*
641 *Chem. Phys.* 7, 2413–2433, 2007.

642 Henze, D. K., Shindell, D. T., Akhtar, F., Spurr, R. J. D., Pinder, R. W., Loughlin, D., Kopacz,
643 M., Sing, K., and Shim, C.: Spatially refined aerosol direct radiative forcing efficiencies.
644 *Environ. Sci. Technol.* 46(17): 9511–18. doi:10.1021/es301993s, 2012.

645 Huang, X., Song, Y., Li, M., Li, J., Huo, Q., Cai, X., Zhu, T., Hu, M. and Zhang, H.: A high-
646 resolution ammonia emission inventory in China, *Global Biogeochemical Cycles*, 26,
647 GB1030, doi:10.1029/2011GB004161, 2012.

648 Kulshrestha, U. C., Granat, L., Engardt, M., and Rodhe, H.: Review of precipitation monitoring
649 studies in India -a search for regional patterns, *Atmospheric Environment*, 39, 4419-4435,
650 2005.

651 Lin, N. H., Tsay, S. C., Maring, H. B., Yen, M.-C., Sheu, G.-C., Wang, S.-H., Chi, K. H.,
652 Chuang, M.-T., Ou-Yang, C.-F., Fu, J. S., Reid, J. S., Lee, C.-T., Wang, L.-C., Wang, J.-L.,
653 Hsu, C. N., Sayer, A. M., Holben, B. N., Chu, Y.-C., Nguyen, X. C., Sopajaree, K., Chen, S.-
654 J., Cheng, M.-T., Tsuang, B.-J., Tsai, C.-J., Peng, C.-M., Schnell, R. C., Conway, T., Chang,

655 C.-T., Lin, K.-S., Tsai, Y. I., Lee, W.-J., Chang, S.-C., Liu, J.-J., Chiang, W.-L., Huang, S.-J.,
656 Lin, T.-H., Liu, G.-R.: An overview of regional experiments on biomass burning aerosols and
657 related pollutants in Southeast Asia: From BASE-ASIA and the Dongsha Experiment to 7-
658 SEAS, *Atmospheric Environment*, 78, 1-19, [doi:10.1016/j.atmosenv.2013.04.066](https://doi.org/10.1016/j.atmosenv.2013.04.066), 2013.

659 Luo, M., Shephard, M. W., Cady-Pereira, K. E., Henze, D. K., Zhu, L., Bash, J. O., Pinder, R.
660 W., Capps, S. L., Walker, J. T., Jones, M. R.: Satellite observations of tropospheric ammonia
661 and carbon monoxide: Global distributions, regional correlations and comparisons to model
662 simulations, *Atmospheric Environment*, 106 (2015) 262e277,
663 [/dx.doi.org/10.1016/j.atmosenv.2015.02.007](https://dx.doi.org/10.1016/j.atmosenv.2015.02.007), 2015.

664 Malm, W. C., Schichtel, B. A., Pitchford, M. L., Ashbaugh, L. L. and Eldred, R. A.: Spatial and
665 monthly trends in speciated fine particle concentration in the United States, *J. Geophys. Res.*,
666 109, D03306, [doi:10.1029/2003JD003739](https://doi.org/10.1029/2003JD003739), 2004.

667 Martin, S. T., Hung, H.-M., Park, R. J., Jacob, D. J., Spurr, R. J. D., Chance, K. V., and
668 Chin, M.: Effects of the physical state of tropospheric ammonium-sulfate-nitrate particles on
669 global aerosol direct radiative forcing, *Atmos. Chem. Phys.*, 4, 183-214, [doi:10.5194/acp-4-](https://doi.org/10.5194/acp-4-183-2004)
670 183-2004, 2004.

671 Nowak, J. B., Neuman, J. A., Kozai, K., Huey, L. G., Tanner, D. J., Holloway, J. S., Ryerson, T.
672 B., Frost, G. J., McKeen, S. A. and Fehsenfeld, F. C.: A chemical ionization mass
673 spectrometry technique for airborne measurements of ammonia, *J. Geophys. Res.*, 112,
674 D10S02, [doi:10.1029/2006JD007589](https://doi.org/10.1029/2006JD007589), 2007.

675 Nowak, J.B., J.A. Neuman, Bahreini, R., Brock, C.A., Middlebrook, A.M., Wollny, A.G.,
676 Holloway, J.S., Peischl, J., Ryerson, T. B., and Fehsenfeld, F.C., Airborne observations of
677 ammonia and ammonium nitrate formation over Houston, TX, *J. Geophys. Res.*, 115,
678 D22304, [doi:10.1029/2010JD014195](https://doi.org/10.1029/2010JD014195), 2010.

679 Nowak, J.B., Neuman, J.A., Bahreini, R., Middlebrook, A.M., Holloway, J.S., McKeen, S. A.,
680 Parrish, D.D., Ryerson, T.B. and Trainer, M.: Ammonia sources in the California South
681 Coast Air Basin and their impact on ammonium nitrate formation, *Geophys. Res. Lett.*, 39,
682 L07804, [doi:10.1029/2012GL051197](https://doi.org/10.1029/2012GL051197), 2012.

683 Oliveras, I., Anderson, L. O. and Malhi Y.: Application of remote sensing to understanding fire
684 regimes and biomass burning emissions of the tropical Andes, *Global Biogeochemical*
685 *Cycles*, 28(4), 480-496, 2014.

686 Pan, L., Gille, J. C., Edwards, D. P., Bailey, P. L. and Rodgers, C. D.: Retrieval of tropospheric
687 carbon monoxide for the mopitt experiment. *J. Geophys. Res.*, 103:32277-32290, 1998.

688 Park, R. J., Jacob, D., Field, B. D., Yantosca, R. M. and Chin M.: Natural and transboundary
689 pollution influences on sulfate-nitrate-ammonium aerosols in the United States: implications
690 for policy, *J. Geophys. Res.*, 109, D15204, doi:10.1029/2003JD004473, 2004.

691 Paulot, F., Jacob, D. J. and Henze, D. K.: Sources and processes contributing to nitrogen
692 deposition: An adjoint model analysis applied to biodiversity hotspots worldwide, *Environ.*
693 *Sci. Technol.*, 47(7), 3226–3233, 2013.

694 Paulot, F. and Jacob, D. J.: Hidden Cost of U.S. Agricultural Exports: Particulate Matter from
695  Ammonia Emissions, *Environ. Sci. Technol.*, 48(2), 903–908, 2014.

696 Paulot, F., Jacob, D. J. Pinder, R. W., Bash, J. O., Travis, K. and Henze, D. K.: Ammonia
697 emissions in the United States, European Union, and China derived by high-resolution
698 inversion of ammonium wet deposition data: Interpretation with a new agricultural emissions
699 inventory (MASAGE_NH3), *J. Geophys. Res. Atmos.*, 119, 4343–4364,
700 doi:[10.1002/2013JD021130](https://doi.org/10.1002/2013JD021130), 2014.

701 Pinder, R. W., Walker, J. T., Bash, J. O., Cady-Pereira, K. E., Henze, D. K., Luo, M., Osterman,
702 G. B. and Shephard, M. W.: Quantifying spatial and seasonal variability in atmospheric
703 ammonia with in situ and space-based observations, *Geophys. Res. Lett.*, 38, L04802,
704 doi:10.1029/2010GL046146, 2011.

705 Pope, C. A., Burnett, R. T., Thun, M. J., Calle, E. E., Krewski, D., Ito, K., and Thurston, G. D.:
706 Lung Cancer, Cardiopulmonary, Mortality, and Long-term Exposure to Fine Particulate Air
707 Pollution, *J. Am. Med. Assoc.*, 287, 1132–1141, 2002.

708 R'Honi, Y., Clarisse, L., Clerbaux, C., Hurtmans, D., Duflot, V., Turquety, S., Ngadi, Y., and
709 Coheur, P.-F.: Exceptional emissions of NH₃ and HCOOH in the 2010 Russian wildfires,
710 *Atmos. Chem. Phys.*, 13, 4171-4181, doi:10.5194/acp-13-4171-2013, 2013.

711 Rienecker, M. M., Suarez, M. J., Gelaro, R., Todling, R., Bacmeister, J., Liu, E., Bosilovich, M.
712 G., Schubert, S. D., Takacs, L., Kim, G.-K., Bloom, S., Chen, J., Collins, D., Conaty, A., da
713 Silva, A., Gu, W., Joiner, J., Koster, R. D., Lucchesi, R., Molod, A., Owens, T., Pawson, S.,
714 Pegion, P., Redder, C. R., Reichle, R., Robertson, F. R., Ruddick, A. G., Sienkiewicz,
715 M., and Woollen, J.: MERRA: NASA's Modern-Era Retrospective Analysis for Research
716 and Applications. *J. Climate*, 24, 3624-3648, doi:10.1175/JCLI-D-11-00015.1., 2011.

717 Rodgers, C. D.: Inverse Methods for Atmospheric Sounding, Theory and Practice, World Sci.,
718 River Edge, N. J., 2000.

719 Rodgers, C. D., and B. J. Connor: Intercomparison of remote sounding instruments, *J. Geophys.*
720 *Res.*, 108 4116, doi:10.1029/2002JD002299, 2003.

721 Roelle and Aneja: Environmental Simulation Chambers: Application to Atmospheric Chemical
722 Processes, Springer, Jan 13, 2006 - Science - 457 pages, 2002.

723 Shephard, M. W., Cady-Pereira, K. E., Luo, M., Henze, D. K., Pinder, R. W., Walker, J. T.,
724 Rinsland, C. P., Bash, J. O., Zhu, L., Payne, V. H., and Clarisse, L.: TES ammonia retrieval
725 strategy and global observations of the spatial and seasonal variability of ammonia, *Atmos.*
726 *Chem. Phys.*, 11, 10743-10763, doi:10.5194/acp-11-10743-2011, 2011.

727 Sommer, S. G., Schjoerring, J. K., Denmead, O. T.: Ammonia Emission from Mineral Fertilizers
728 and Fertilized Crops, *Advances in Agronomy*, Vol. 82, pp. 557-622, 2004.

729 Strow, L., Hannon, S., Machado, S., Motteler, H. and Tobin, D.: An Overview of the AIRS
730 Radiative Transfer Model, *IEEE Trans. on Geosci. Remote Sensing*, Vol. 41, pp. 303-313,
731 2003.

732 Susskind, J., Barnett, C. D. and Blaisdell, J. M.: Retrieval of atmospheric and surface parameters
733 from AIRS/AMSU/HSB data in the presence of clouds, *IEEE Trans. on Geosci. Remote*
734 *Sensing*, Vol. 41, pp. 390-409, 2003.

735 Sutton, M., Erisman, J., Dentener, F. and Moller, D.: Ammonia in the environment: From ancient
736 times to the present, *Environ. Pollut.*, 156, 583–604, doi:10.1016/j.envpol.2008.03.013, 2008.

737 Sutton, M. A., Nemitz, E., Erisman, J. W., Beier, C., Bahl, K. B., Cellier, P., de Vries, W.,
738 Cotrufo, F., Skiba, U., Di Marco, C., Jones, S., Laville, P., Soussana, J. F., Loubet, B., Twigg,
739 M., Famulari, D., Whitehead, J., Gallagher, M. W., Neftel, A., Flechard, C. R., Herrmann, B.,
740 Calanca, P. L., Schjoerring, J. K., Daemmgen, U., Horvath, L., Tang, Y. S., Emmett, B. A.,
741 Tietema, A., Penuelas, J., Kesik, M., Brueggemann, N., Pilegaard, K., Vesala, T., Campbell,
742 C. L., Olesen, J. E., Dragosits, U., Theobald, M. R., Levy, P., Mobbs, D. C., Milne, R.,
743 Viovy, N., Vuichard, N., Smith, J. U., Smith, P., Bergamaschi, P., Fowler, D. and Reis, S.:
744 Challenges in quantifying biosphere-atmosphere exchange of nitrogen species, *Environ.*
745 *Pollut.*, 150(1), 125–139, doi:10.1016/j.envpol.2007.04.014, 2007.

746 Updyke, K. M., Nguyen, T. B. and Nizkorodov, S. A.: Formation of brown carbon via reactions
747 of ammonia with secondary organic aerosols from biogenic and anthropogenic precursors,
748 *Atmospheric Environment*, 63, 22-31, 2012.

749 Walker, J. M., Philip, S., Martin, R. V. and Seinfeld, J. H.: Simulation of nitrate, sulfate, and
750 ammonium aerosols over the united states, *Atmos. Chem. Phys.*, 12(22), 11,213–11,227,
751 doi:10.5194/acp-12-11213-2012, 2012.

752 Wang, J., Jacob, D. J. and Martin, S. T.: Sensitivity of sulfate direct climate forcing to the
753 hysteresis of particle phase transitions, *J. Geophys. Res.*, 113, D11207,
754 doi:10.1029/2007JD009368, 2008.

755 Warner, J. X., Carminati, F., Wei, Z., Lahoz, W., Attié, J.-L.: Tropospheric carbon monoxide
756 variability from AIRS and IASI under clear and cloudy conditions, *Atmos. Chem. Phys.*
757 *Discuss.*, 13, 16337-16366, doi:10.5194/acpd-13-16337-2013, 2013.

758 Warner, J. X., Wei, Z., Strow, L. L., Barnet, C. D., Sparling, L. C., Diskin, G., Sachse, G.:
759 Improved Agreements of AIRS Tropospheric Carbon Monoxide Products with Other EOS
760 Sensors Using Optimal Estimation Retrieval, *Atmos. Chem. Phys.*, 10, 9521-9533,
761 doi:10.5194/acp-10-9521-2010, 2010.

762 Warner, J. X., Comer, M. M., Barnet, C. D., McMillan, W. W., Wolf, W., Maddy, E., Sachse,
763 G.: A Comparison of Satellite Tropospheric Carbon Monoxide Measurements from AIRS
764 and MOPITT During INTEX-A, *J. Geophys. Res.*, doi:10.1029/2006JD007925, 2006.

765 Wu, S.-Y., Krishnanb, S., Zhang, Y., Aneja, V.: Modeling atmospheric transport and fate of
766 ammonia in North Carolina—Part I: Evaluation of meteorological and chemical predictions,
767 *Atmospheric Environment*, 42 (2008) 3419–3436, 2007.

768 Yamaji, K., Ohara, T. and Akimoto, H.: Regional-specific emission inventory for NH₃, N₂O,
769 and CH₄ via animal farming in south, southeast, and East Asia, *Atmospheric Environment*,
770 38(40), 7111-7121, 2004.

771 Yevich, R., and Logan, J. A.: An assessment of biofuel use and burning of agricultural waste in
772 the developing world, *Global Biogeochem. Cycles*, 17(4), 1095, doi:10.1029/2002GB001952,
773 2003.

774 Zhu, L., Henze, D. K., Cady-Pereira, K. E., Shephard, M. W., Luo, M., Pinder, R. W., Bash, J. O.
775 and Jeong, G.-R.: Constraining U.S. ammonia emissions using TES remote sensing

776 observations and the GEOS-Chem adjoint model, J. Geophys. Res. Atmos.,
777 doi:10.1002/jgrd.50166, 2013.

778

779 **Figure Captions:**

780

781 **Fig.1.** The *a priori* profiles and the square root of the diagonal terms of the error covariance
782 matrices for the low emission levels (left panel), the moderate emission levels (middle panel),
783 and the high emission levels (right panel), respectively.

784

785 **Fig. 2.** Correlation between the DBTI (Difference of Brightness Temperature Index) and DOFS
786 (Degrees Of Freedom for Signal) for the three emission levels with low emissions in blue,
787 moderate emissions in green, and high emissions in red.

788

789 **Fig. 3.** AIRS NH₃ validation against CRDS (the cavity ring down spectrometer) spiral profiles
790 collected during the DISCOVER-AQ CA (01/16-02/06, 2013). The red curves represent AIRS
791 retrieved profiles, gray curves are the *a priori* profiles, green solid lines are *in situ* spiral profiles,
792 and the blue dashed lines are the convolved profiles using AIRS NH₃ AKs. The x-axis is linear
793 from 0 to 25 ppbv and logarithmic from 25 to 150 ppbv.

794

795 **Fig. 4.** Upper panel: AIRS global NH₃ VMRs at 918 hPa, averaged from September 2002
796 through August 2015. The colorbar is linear from 0 to 5 ppbv and 5 to 10 ppbv, but with
797 different increments. Lower panel: The total occurrences (number of days) of high emissions
798 (VMRs > 1.0 ppbv at 918 hPa) in the 13-year period. Red/blue indicate relatively high/low
799 occurrences of high emissions, respectively.

800

801 **Fig. 5.** AIRS NH₃ DOFS values averaged over September 2002 – August 2015 period. Red/blue
802 indicate relatively high/low DOFS, respectively.

803

804 **Fig. 6.** Top panel: The NH₃ VMRs from the persistent sources filtered with the collocated
805 occurrences of elevated emissions (≥ 1.4 ppbv) using a threshold of 40 d Middle panel:

Juying Warner 4/6/16 9:45 AM


Deleted: green

Juying Warner 4/6/16 9:44 AM


Deleted: x-axis

808 Pasture and Cropland Map (<http://OurWorldInData.org>); and Bottom panel: irrigated agricultural
809 land areas (data.worldbank.org).

810

811 **Fig. 7.** AIRS NH₃ VMRs at 918 hPa averaged between September 2002 and August 2015 for
812 December-January-February (DJF, upper left panel), March-April-May (MAM, upper right
813 panel), June-July-August (JJA, lower left panel), and September-October-November (SON,
814 lower right panel), with DOFS greater than 0.1 and no cutoff limit for the VMRs. Red/pur 
815 indicate relatively high/low NH₃ VMRs.

816

817 **Fig. 8.** As in Fig. 7 except for the occurrences of high emissions (VMRs ≥ 1 ppbv). Red/b 
818 indicate relatively high/low occurrences of high emissions.

819

820 **Fig. 9.** The NH₃ monthly mean variations (solid line) in the NH (upper panel) and the SH (lower
821 panel), respectively. The long-dash lines show the 1 σ standard deviation (STD); and the shaded
822 areas represent the maximum and minimum range of each dataset.

823

824 **Footnotes for Figure 6:**

825

826 [The World Bank provided the statement that the maps displayed on the World Bank web site are](#)
827 [for reference only and do not imply any judgment on the legal status of any territory, or any](#)
828 [endorsement or acceptance of such boundaries.](#)